Low Temperature Physics/Fizika Nizkikh Temperatur, 2019, v. 45, No. 5, pp. 576–583

Tunneling conductance of the *s*-wave and *d*-wave pairing superconductive graphene–normal graphene junction

A.M. Korol

National University for Food Technologies, Volodymyrska Str. 68, Kyiv 01601, Ukraine
Laboratory on Quantum Theory in Linkoping, ISIR, P.O. Box 8017, S-580, Linkoping, Sweden
E-mail: korolam@ukr.net

Received December 7, 2018, revised January 14, 2019, published online March 26, 2019

Within the framework of the Blonder–Tinkham–Klapwijk formalism we calculate and analyze the conductance of the normal graphene — *s*-wave and independently *d*-wave pairing superconductive graphene junction. The eigenfunctions, the Andreev and the normal reflection rates are obtained by solving the Dirac–Bogoliubov–de Gennes equations. The Fermi velocity is believed to be different in the normal and in the superconductive regions. We consider the options of gapless and gapped graphene for both cases: *s*-wave and independently *d*-wave pairing. It is demonstrated that the characteristics of the junction considered are sensitive to the ratio v_{FN}/v_{FS} where v_{FN}, v_{FS} are the Fermi velocities in the normal and the superconductive graphene respectively. This conclusion refers to the Andreev reflection as well as to the normal one. The first of them is shown to be the dominant process for the formation of the conductivity. These results are true for an arbitrary value of the orientational angle of the *d*-waves. Each of four cases considered: *s*-, *d*-wave pairing and gapless and gapped graphene displays its own specific features of the conductance. The dependence of the conductance on the external electrostatic potential as well as on the Fermi energy is also analyzed in every case. The obtained results may be useful for controlling the transport properties of the normal graphene–superconductive graphene junction.

Keywords: graphene–superconductive graphene junction, Andreev and normal reflections, conductance, Fermi velocity.

1. Introduction

Recently, the researchers close attention was focused on the so-called Dirac materials ([1] and references therein). These include some various and diverse substances such as graphene, topological insulators, *d*-wave high-temperature superconductors, superfluid phase ^{3}He etc. (see the corresponding table in [1]). The unifying factor for them is that their low-energy fermion excitations are subjected to the Dirac equation, and the dispersion relation of quasiparticles is linear in nature. As a result, Dirac materials have many common features [1]. It should also be emphasized that the Dirac materials will be of great practical importance, since some of their properties are robust against external perturbations due to, in particular, symmetry with respect to the inversion of time [1]. The key value that characterizes the dispersion relation of the Dirac quasiparticles is the Fermi velocity. Therefore, it is clear that significant efforts have been made to be able to control this value and also to use this control in practice [2–12]. For this purpose, a number of different methods were proposed and experimentally tested. The Fermi velocity of charge carriers in various structures is made to vary in space by some special techniques, e.g., by the appropriate doping [3], placing a grounded metal plane close to graphene sheet (which makes electron-electron interactions weaker and thereby modifies the Fermi velocity) [2], stretching a small region of a graphene sheet [4] and others.

As graphene is one of the Dirac materials much attention has been paid to the study of graphene and various graphene-based structures in recent years. This is due to nontrivial properties of graphene such as a linear dispersion relation for the quasiparticles, whose behavior at low energies is described by an equation similar to the Dirac–Weyl one, unusual quantum Hall effect, the property of chirality, the Klein tunneling, high mobility, ballistic transport etc. [4]. And it should also be borne in mind that graphene is a promising material for modern electronics. One of the priority directions is to study the various possibilities of controlling the energy spectrum of the graphene-based structures. The electron-wave propagation in the graphene-based structures with the tunable Fermi velocity was investigated in [2–12] including the effect of the magnetic and the electric field. At the same time the pristine graphene can also be induced by the external forces to become the superconducting material, for example, super-

conductivity can be induced in a graphene layer in the presence of a superconducting electrode near it due to the proximity effect. That's why a lot of works were devoted to exploring of the properties of such structures as the superconductive graphene, graphene–superconductive graphene, graphene–insulator–superconductive graphene, graphene-based Josephson junctions [13–25]. However, the effect of tuning of the Fermi velocity on the characteristics of these contacts has not been investigated so far. The Fermi velocity values were assumed to be equal in every region of the structure considered in all of the cited references. From the above, it follows the importance of the problem of analyzing the transport features of charge carriers in the junction: normal graphene–superconducting graphene due to different values of the Fermi velocity in the normal and superconducting parts of the contact. The present work is devoted to this analysis. Both the gapless and the gapped graphene are taken into consideration.

Also we would like to note that one can find in literature a large variety of pairing models used in different junctions which include the superconductive regions (the junctions may not contain graphene as their part, obviously): *s*-, *d*-, *p*-, *f*-, *g*-, and other models of wave pairing (see, e.g., [13–34]). The Fermi velocity is believed to be equal in every region of the considered junctions in all cited references. But, firstly, it may not be so in fact and, secondly, one can change the Fermi velocity value in one or another junction region specially (see, e.g., [2–12]). The main goal of the present work is to show, in the relatively simple models, that it is possible to control effectively the transport properties of the related junctions by tuning the Fermi velocity values in one or another junction region. For this purpose we use the relatively simple models of *s*-wave (as for example in [14,16,20,21,33]) and independently *d*-wave (as, e.g., in [15,16,23]) pairing.

The paper is organized as follows. Section 2 presents the considered model and needed formulae and we discuss the results of calculations for the cases of the *s*- and *d*-pairing in Sects. 3, 4, respectively.

2. Model and formulae

Let the normal and the superconductive parts of the junction studied be placed along the 0*x* axis so that their interface locates at a point $x = 0$. Let the superconducting order parameter has the form (*s*-wave pairing, as for example, in [14,16,20,21,33]):

$$\Delta_s = \mathrm{e}^{i\varphi}\Delta_0 \vartheta(x) \tag{1}$$

where φ is the superconductive phase, $\vartheta(x)$ is the Heaviside unit step function. The eigenfunctions which describe the quasiparticle in this system are subjected to the Dirac–Bogolyubov–de Jennes equation

$$\begin{bmatrix} H - U(x) & \Delta_s(x) \\ \Delta_s^*(x) & -H + U(x) \end{bmatrix} \Psi(x) = E\Psi(x) \tag{2}$$

where $H = -ihv_F(\sigma_x\partial_x + \sigma_y\partial_y)$ is the Dirac Hamiltonian, U the external electrostatic potential applied to the superconducting region (it is believed that an additional electrode covers the superconductor region), v_F is the Fermi velocity, σ_x, σ_y are Pauli matrices for the pseudospin. The solution of the equation (2) is the four-component electron and hole spinors which are of the following form: in NG region

$$\Psi_N(x) = \begin{pmatrix} 1 \\ \mathrm{e}^{i\Theta_N} \\ 0 \\ 0 \end{pmatrix} \mathrm{e}^{ik_{Ne}x} + r_n \begin{pmatrix} 1 \\ -\mathrm{e}^{-i\Theta_N} \\ 0 \\ 0 \end{pmatrix} \mathrm{e}^{-ik_{Ne}x} + r_a \begin{pmatrix} 0 \\ 0 \\ 1 \\ e^{i\Theta_N} \end{pmatrix} \mathrm{e}^{-ik_{Nh}x}, \tag{3}$$

in SG region

$$\Psi_S(x) = t \begin{pmatrix} 1 \\ \mathrm{e}^{i\Theta_S} \\ \mathrm{e}^{-i\beta}\mathrm{e}^{-i\varphi} \\ \mathrm{e}^{i\Theta_S}\mathrm{e}^{-i\beta}\mathrm{e}^{-i\varphi} \end{pmatrix} \mathrm{e}^{ik_S x - kx} + t' \begin{pmatrix} 1 \\ -\mathrm{e}^{-i\Theta_S} \\ \mathrm{e}^{i\beta}\mathrm{e}^{-i\varphi} \\ -\mathrm{e}^{-i\Theta_S}\mathrm{e}^{i\beta}\mathrm{e}^{-i\varphi} \end{pmatrix} \mathrm{e}^{-ik_S x - kx}, \tag{4}$$

$$k_{Ne(h)} = \frac{\cos\Theta_{Ne(h)}}{v_{FN}} \sqrt{\left[E_F + (-)E\right]^2 - \Delta_N^2},$$

$$k_S = (E_F + U)\frac{\cos\Theta_S}{v_{FS}},$$

$$k_S = (E_F + U)\frac{\cos\Theta_S}{v_{FS}},$$

$$k^{-1} = \frac{v_{FS}^2 k_S}{(U + E_F)\Delta_S \sin\beta},$$

$$\beta = \cos^{-1}\left(\frac{E}{\Delta_S}\right) \text{ if } |E| < \Delta_S,$$

$$\beta = -i\mathrm{ch}\left(\frac{E}{\Delta_S}\right) \text{ if } |E| > \Delta_S.$$

Units $\hbar = v_0 = 1$ are adopted, v_0 being the Fermi velocity in the pristine graphene; we use the dimensionless units for the Fermi velocity $v_F \to v_F / v_0$, and present the energy quantities in meV for convenience.

Angles of incidence of the quasiparticle wave on the normal and the superconductive regions of the junction considered are associated by the following equality

$$k_N \sin\Theta_N = k_S \sin\Theta_S . \qquad (5)$$

(The analogous to (1)–(5) formulae have been widely used in literature, e.g., in the papers [13–23]).

The coefficients in (3), (4) can be found by applying the following appropriate boundary conditions on the eigenfunctions

$$\sqrt{v_{FN}}\,\Psi_N\left(x=0\right) = \sqrt{v_{FS}}\,\Psi_S\left(x=0\right), \qquad (6)$$

(see, e.g., [2,3,5–10]).

As a result we obtain for the coefficients of the Andreev and normal reflections the expressions which are given in the Appendix.

The conductivity G of the junction investigated can be calculated due to known Blonder–Tinkham–Klapvijk formalism [35] which expresses G in terms of r_a and r_n:

$$G\left(E,E_F,U\right) = G_0 \int_0^{\frac{\pi}{2}} \left[1+\left|r_a\left(E,\Theta_N,E_F,U\right)\right|^2 - \right.$$

$$\left. - \left|r_n\left(E,\Theta_N,E_F,U\right)\right|^2\right]\cos\left(\Theta_N\right) d\Theta_N \qquad (7)$$

where G_0 is the ballistic conductivity of the normal graphene. The equation (7) yields the conductivity of the structure under consideration for arbitrary parameter values.

3. Results and discussion for the case of *s*-wave pairing

Figure1 shows the dependence of the normalized (dimensionless) conductivity $G^* = G/G_0$ on the dimensionless energy of quasiparticles $E' = E/\Delta_0$ in the case in which a normal part of the considered contact is the gapless graphene ($\Delta_N = 0$). The upper and the lowest curves in r_a (E) and $G^*(E')$ dependences correspond to the values of the Fermi velocity in the superconductor equal to 1 and 2 respectively, the third curve refers to $v_{FS} = 1.5$; for the r_n (E') dependence the upper and the lowest curves refer to $v_{FS} = 2$ and 1 respectively. (We put an angle of incidence of the quasiparticle wave on the normal region to be equal to $\pi/6$ throughout the text, the superconductive parameter Δ_0 = 12 meV [4]).

As follows from references [2,3,5–10] the magnitude of the Fermi velocity may vary approximately up to 4 in relation to this value in the pristine graphene. Curve *1* shows that the calculations of our work are in agreement with the results of the previous studies [13–23] according to which conductivity G^* is not dependent on energy E in the range where it does not exceed the size of the superconducting gap. However, we see that in the case of different values of the Fermi velocity v_{FN} and v_{FS} the dependence of conductivity on the excitation energy of quasiparticles in the above energy range $0 < E < \Delta_S$ takes place. This result is qualitatively different from that obtained in papers [13–23] and it shows that the value of the conductivity of the system under investigation depends on energy E throughout its whole range.

The larger is the difference between the Fermi velocities in the normal and the superconductor areas, the more substantial effect on the conductivity we observe. For all the cases considered in which $v_{FS} \neq v_{FN}$, the magnitude of conductivity has a peak-like maximum at a point $E = \Delta_S$; the maximum value of G^* grows with v_{FS} decreasing (if

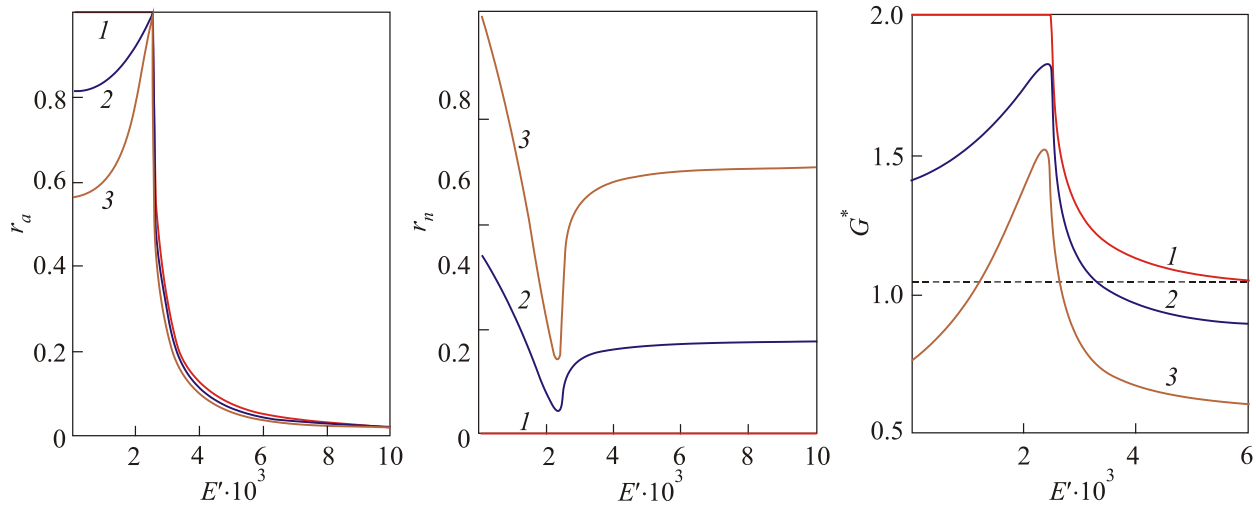

Fig. 1. Functions of $r_a(E')$, $r_n(E')$, $G^*(E')$ for the gapless normal region of the junction considered ($\Delta_N = 0$). The upper and the lowest curves in r_a (E) and $G^*(E')$ correspond to the values of the Fermi velocity in the superconductor equal to 1 and 2 respectively, the third curve refers to $v_{FS} = 1.5$; for the r_n (E') dependence the upper and the lowest curves refer to $v_{FS} = 2$ and 1, respectively.

$v_{FS} > v_{FN}$).

Consider further the results obtained for contacts: the gapped normal graphene–superconducting graphene. First of all, note that the conductivity of this system G^* reveals a complicated dependence on its parameters and the results of calculation of G^* essentially depends on the interplay between the parameters such as the Fermi velocity in the normal and the superconducting regions (ratio v_{FS}/v_{FN}), the magnitude of a gap in the normal area Δ_N, an external electrostatic potential U, the Fermi energy E_F. As for the case of $\Delta_N = 0$ the larger is the difference between the Fermi velocities in the normal and the superconductor areas, the more substantial effect on the conductivity we observe.

Note also that the examined characteristics of the NG–NS contact containing the gapped graphene in the N region have some quality differences from the case of a contact with the gapless graphene. So in the former case, there is a significant functional dependence of conductivity on the potential U, as well as on the Fermi level E_F, while the conductivity of the system which includes the gapless graphene is independent of variables U and E_F. Because of this, in particular, in subsequent figures, we present the results of our calculations for two different values of U, namely $U_1 = 0$ and $U_2 = 5.6$ eV.

Figure 2 shows the dependence of the normal, of the Andreev reflection, and of the dimensionless conductivity G^* on the excitation energy for NG–NS contact for the following parameters: Fermi velocity in N region $v_{FN} = 1$; the gap width in N region 56 meV, the upper and the lower curves in this figure correspond to values of potential U: $U_1 = 0$ and $U_2 = 5.6$ eV $v_{FS} = 1.5$. It is evident that the functions $r_a(E)$ and $r_n(E)$, i.e., the rates of the Andreev and the normal reflection respectively have the peak-like extremes at a point $E = \Delta_S$, which is equal to the width of the superconducting gap. It is true for arbitrary values of the potential U. However, the behavior of the Andreev and the normal reflection rates has the opposite character, namely the function $r_a(E)$ increases with energy from zero and reaches a maximum at a point $E = \Delta_S$; instead the function $r_n(E)$ decreases with E increasing, reaches a minimum value at a point $E = \Delta_S$, and then grows. The value of conductivity $G^*(E)$ is mainly determined by the Andreev reflection process and the shape of the corresponding curve is similar to that of the function $r_a(E)$. We would like to emphasize here two important facts: 1) conductivity depends on the potential U (unlike for the case where $\Delta_N = 0$, $v_{FN} = 1$; 2) increasing in potential U leads to higher values of the conductivity unlike for the case of identical Fermi velocity values in N and S contact regions ($v_{FS} = v_{FN} = 1$, $\Delta_N \neq 0$). This behavior is due to the process of the Andreev reflection. Note also that the conductance increases with decreasing of the Fermi velocity in the superconducting region v_{FS}.

Figure 3 presents the same functions as in Fig. 2, but for the case of bigger gap in the normal region Δ_N = 112 meV. For larger values of Δ_N, there is an interesting result: the conductivity reveals the non-monotonic dependence on the Fermi velocity values in the superconductors region v_{FS}. In this case, contrary for the case of smaller values Δ_N the conductivity increases with increasing v_{FS}, then reaches its maximum at the value v_{FS} which is approximately equal to 1.6, then G^* is reduced. This behavior of the conductivity as a function of the Fermi velocity is again due the process of Andreev reflection.

Regarding the dependence of the Andreev, of the normal reflections and of the conductivity on the Fermi energy E_F we would like to note the main features of these relationships which are as follows:

1) unlike for the case of $\Delta_N = 0$, $v_{FN} = 1$ these functions depend essentially on the Fermi level E_F;

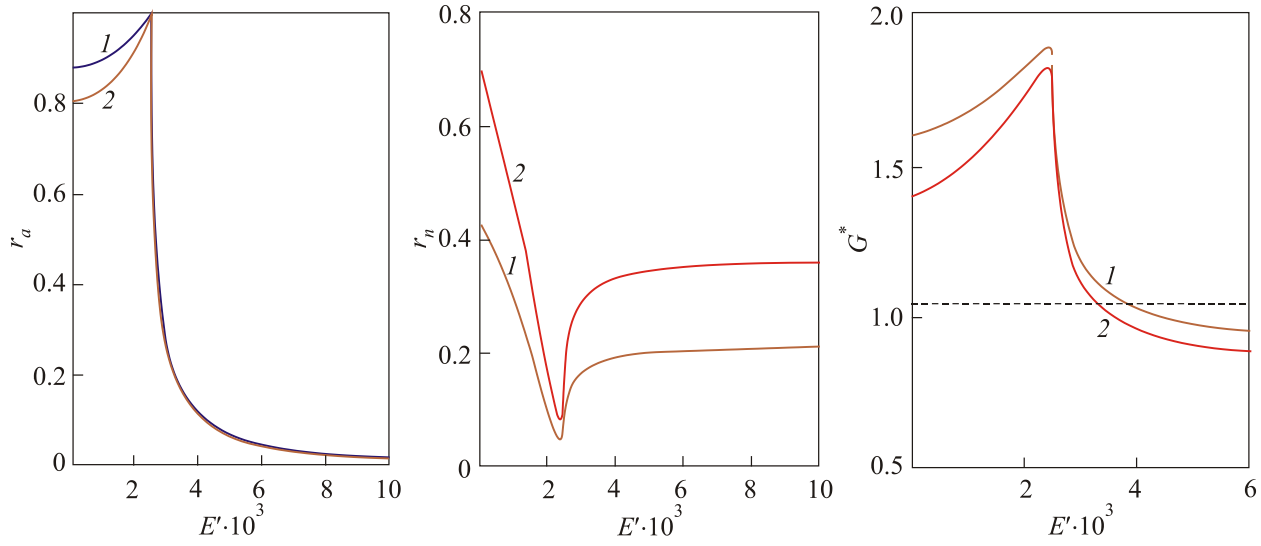

Fig. 2. Plots of $r_a(E')$, $r_n(E')$, $G^*(E')$ dependencies for the gapped normal region with the values of ΔN = 56 meV, $v_{FS} = 1.5$. The upper and the lower curves in this figure correspond to values of potential U: $U_1 = 0$ and $U_1 = 5.6$ eV, respectively.

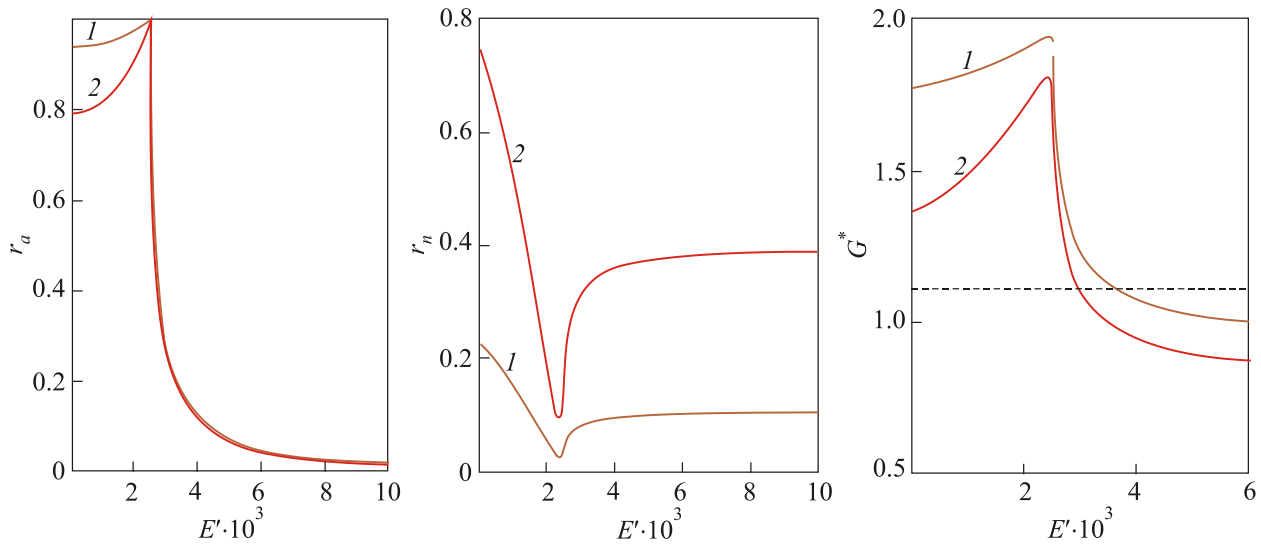

Fig. 3. Plots of the Andreev, of the normal reflections and of the conductivity dependencies on energy for the values of Δ_N = 112 meV, $v_{FS} = 1.5$. The upper and the lower curves in this figure correspond to values of potential U: $U_1 = 0$ and $U_2 =$ 5.6 eV, respectively.

2) decreasing in E_F leads to the increased conductivity and not to its decreasing as for the case $v_{FN} = 1$, $\Delta_N \neq 0$.

3) functions $r_a(E')$, $r_n(E')$, $G^*(E')$ become practically independent on U for sufficiently large values of E_F.

4. Results and discussion for the case of *d*-wave pairing.

Now we consider the case of the *d*-wave pairing and modeled it with the help of the so called $d_{(x^2-y^2)}$ model so that the superconducting order parameter is of the form (as e.g., in [15,16,23]):

$$\Delta_s = e^{i\varphi}\Delta_0 \cos(2\Theta_S - 2\alpha)\vartheta(x) \qquad (8)$$

where $\vartheta(x)$ is the Heaviside unit step function, φ is the superconductive phase, Θ_S angle of incidence of the quasiparticles, α the rotational angle. We put an angle of incidence of the quasiparticle wave on the normal region to be equal to $\pi/6$, the superconductive parameter Δ_0 = 12 meV [4].

Note that as in the case of *s*-wave pairing conductivity of this system G^* displays a complicated dependence on its parameters and the results of calculation of G^* essentially depends on the interplay between the following parameters: the rotational angle, the Fermi velocity in the normal and the superconducting regions, the magnitude of a gap in the normal area Δ_N, an external electrostatic potential U, the Fermi energy E_F.

Figure 4 shows the dependence of the normalized (dimensionless) conductivity $G^* = G/G_0$ on the dimensionless energy of quasiparticles $E' = E/\Delta_0$ in the case in which a normal part of the considered contact is the gapped graphene, $\Delta_N = 56$ mV the value of the rotational angle α is equal to $\pi/6$.

As in the case of s-pairing there is a significant functional dependence of conductivity on the potential U, as well as on the Fermi level E_F, so, in subsequent figures, we present the results of our calculations for two different values of U, namely $U_1 = 0$ and $U_2 = 5.6$ eV. (Note that the conductivity of the system which includes the gapless graphene is independent of variables U and E_F). It is seen from Fig. 4 that the conductivity of the structure explored has the peak-like extremes not at the energy point equal to the width of the superconducting gap $E = \Delta_0$, as it is for the case of the s-wave symmetry, but there is a substantial shift of this peak to lesser excitation energies due to the nonzero value of α. It is true for arbitrary values of the potential U. The value of conductivity $G^*(E)$ is mainly determined by the Andreev reflection process and the shape of the corresponding curve is similar to that of the function $r_a(E)$ —

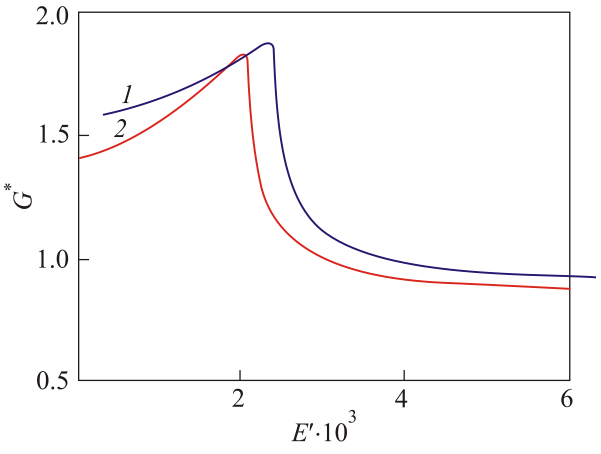

Fig. 4. The dependence of the normalized (dimensionless) conductivity $G^* = G/G_0$ on the dimensionless energy of quasiparticles $E' = E/\Delta_0$, values of Δ_N = 56 meV, $v_{FS} = 1.5$, $\alpha = \pi/6$. The upper and the lower curves in this figure correspond to values of potential U: $U_1 = 0$ and $U_2 =$ 5.6 eV, respectively, E_F = 0.56 eV.

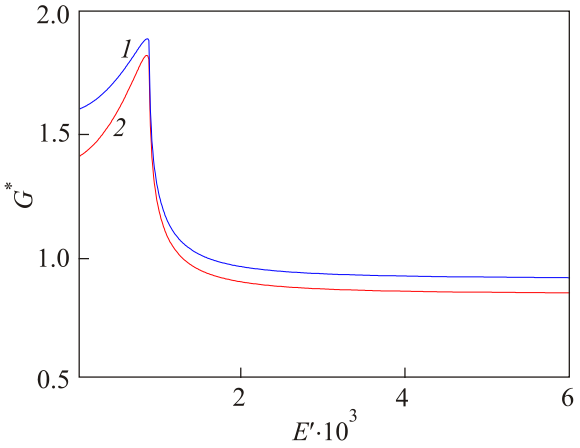

Fig. 5. The dependence of the conductivity on energy for $\alpha = \pi/4$, $\Delta_N = 56$ meV, $v_{FS} = 1.5$. The upper and the lower curves refer to values of $U = 0$; 5.6 eV respectively, $E_F = 0.56$ eV.

as for the case of the *s*-wave pairing.

The upper and the lower curves in this figure correspond to values of potential U: namely $U_1 = 0$ and $U_2 = 5.6$ eV, respectively, $E_F = 0.56$ eV.

Figure 5 presents the conductivity as a function of energy for the value of α which is equal to $\pi/4$. Here the shift of the maximum peak is essentially larger than for the case of $\alpha = \pi/6$: hence the shift of the observed curves is very sensitive to values of the rotational angle in the *d*-wave pairing.

Figure 6 presents the G^* vs E function for the following values of the difference between the Fermi velocities in the normal and the superconductor areas: $v_{FS} = 1.2$, $\alpha = \pi/6$ (Fig. 6(a)), and $v_{FS} = 2$, $\alpha = \pi/4$ (Fig. 6(b)), $\Delta_N = 56$ meV. We see from Figs. 4–6 that the larger is the difference between the Fermi velocities in the normal and the superconductor areas, the more substantial effect on the conductivity we observe. For all the cases considered in which $v_{FS} \neq v_{FN}$, the magnitude of conductivity has a peak-like maximum at a point that depends on the value of α; the maximum value of G^* grows with v_{FS} decreasing independently on α (if $v_{FS} > v_{FN}$).

In Fig. 7 the function $G^*(E)$ is plotted for the case of bigger gap in the normal region $\Delta_N = 112$ meV. As for *s*-wave pairing, for larger values of Δ_N, an interesting result is observed: the conductivity reveals the non-monotonic dependence on the Fermi velocity values in the superconductors region v_{FS}. In this case, contrary for the case of smaller values Δ_N the conductivity increases with increasing v_{FS}, then reaches its maximum at the value v_{FS} which is approximately the same for different values of α, then lessens.

And we see that not only the location of the maximum essentially depends on α but the magnitude of the conductivity also is substantially dependent on the rotational angle value.

Next we would like to note that the function $G^*(E)$ depends substantially on E_F and it is true for an arbitrary

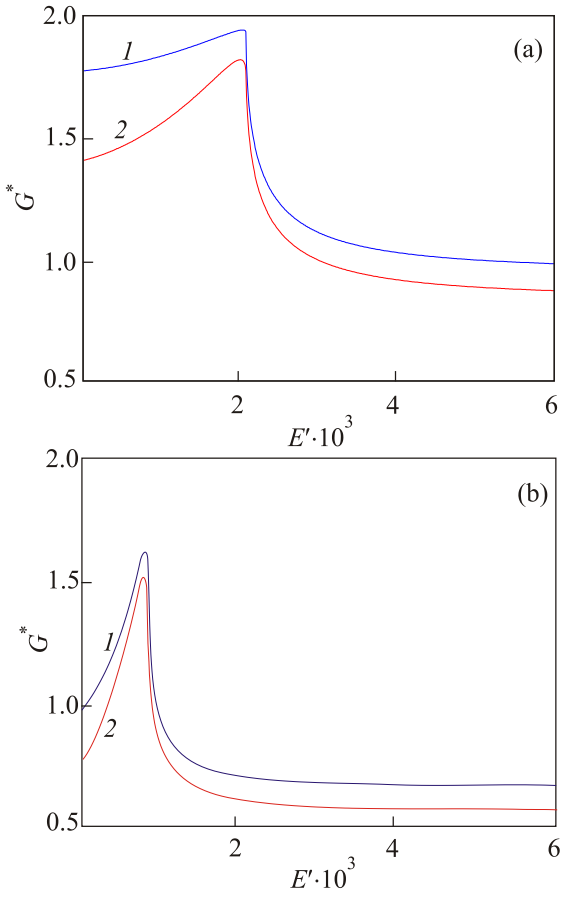

Fig. 6. The dependence of the conductivity on energy for the following values of the difference between the Fermi velocities in the normal and the superconductor areas: $v_{FS} = 1.2$, $\alpha = \pi/6$ (a), $v_{FS} = 2$, $\alpha = \pi/4$ (b), $\Delta_N = 56$ meV. The upper and the lower curves in Figs. 6(a) and (b) correspond to values of potential U: $U_1 = 0$ and $U_2 = 5.6$ eV, respectively, $E_F = 0.56$ eV.

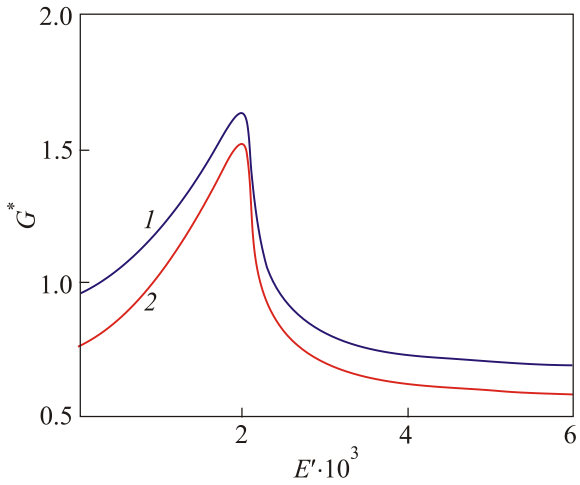

Fig. 7. The dependence of the conductivity on energy for the case of bigger gap in the normal region $\Delta_N = 112$ meV, $\alpha = \pi/6$, $v_{FS} = 1.5$. The upper and the lower curves correspond to values of potential U: $U_1 = 0$ and $U_2 = 5.6$ eV, respectively, $E_F = 0.56$ eV.

value of α. Decreasing in E_F leads to the increased conductivity and not to its decreasing as for the case $v_{FS} = 1$, $\Delta_N \neq 0$. The conductivity becomes practically independent on U for sufficiently large values of E_F.

Considering the case of the junction studied with the gapless normal graphene we must note the following. Independently of values of α the conductivity does not depend on energy in the region where $E < \Delta_S$ — as for the case of *s*-pairing. The larger is the difference between the Fermi velocities in the normal and the superconductor areas, the more substantial effect on the conductivity we observe for each value of α. As for the case of the gapped normal graphene, for all the cases considered in which $v_{FS} \neq v_{FN}$, the magnitude of conductivity has a peak-like maximum at a point $E = \Delta_S$; the maximum value of G^* grows with v_{FS} decreasing (if $v_{FS} > v_{FN}$). The function $G^*(E)$ is independent on the external potential U for the case $\Delta_N = 0$, $v_{FS} \neq 1$.

5. Conclusions

The following nanoscale structure is considered: the *s*-, and independently *d*-wave pairing superconducting graphene in contact with the normal graphene. It is believed that the Fermi velocity value in the superconducting graphene may differ from that in the pristine graphene. With the help the Blonder–Tinkham–Klapwijk formalism, the conductivity G is calculated taking into account the fact that the external potential U is applied to the superconducting part of the given structure. The coefficients of both the normal and the Andreev reflection are evaluated within the framework of the Dirac–Bogoliubov–de Gennes equations. It is shown that the determining factor in the formation of the conductivity is the process of Andreev reflection. A characteristic feature of the $G(E)$ dependence is the presence of a peak at the energy point $E = \Delta_S$, Δ_S being the superconducting energy gap in graphene which depends in particular on the value of the rotational angle. The value of the maximum (peak) value of $G(E)$, as well as the $G(E)$ curve steepness essentially depends on the value of the Fermi velocity v_F. The dependence of the conductivity on the potential U as well as on the Fermi level E_F is analyzed for different values of the rotational angle. The obtained results of the present work may be useful for controlling the conductivity of the considered junction due to changing of the Fermi velocity in each of the junction regions. And we would like to emphasize that this statement can be related to a lot of other junctions containing the normal and the superconductive regions, such as considered in, for example, [27–34].

Appendix A

Expressions for the Andreev and the normal reflections are as follows:

$$r_a = \frac{v u e^{-i\varphi} ab}{j}, \quad r_n = c\left[\frac{cu^2 + dv^2}{j}\right] - 1,$$

$$a = q + l,\ b = l + p,\ c = q - l,\ d = n - l,\ j = u^2 ef - v^2 gh,$$

$$h = l + n,\ e = q + n,\ f = l - p,\ g = q - p.$$

$$l = \frac{E_F - \Delta_N}{\sqrt{v_{FN} v_{FS}}\, k_N} e^{i\Theta_N},\quad q = \frac{E_F - \Delta_N}{\sqrt{v_{FN} v_{FS}}\, k_N} e^{-i\Theta_N},$$

$$n = \frac{E_F + U - \Delta_S}{\sqrt{v_{FN} v_{FS}}\, k_S} e^{i\Theta_S},\quad p = \frac{E_{FN} + U - \Delta_S}{\sqrt{v_{FN} v_{FS}}\, k_S} e^{-i\Theta_S}.$$

$$u(E) = \sqrt{0{,}5\left(1 + \frac{\Omega(E)}{E}\right)},\quad v(E) = \sqrt{0.5\left(1 - \frac{\Omega(E)}{E}\right)},$$

$$\Omega(E) = \sqrt{E^2 - \Delta_S^2},$$

and we account for the condition $E_F,\ \Delta_N \gg E$.

1. T.O. Wehling, A.M. Black-Schaffer, and A.V. Balatsky, *Adv. Phys.* **63**, 1 (2014).
2. A. Raoux, M. Polini, R. Asgari, A.R. Hamilton, R. Fasio, and A.H. MacDonald, *Phys. Rev. B* **81**, 073407 (2010).
3. L. Tapashto, G. Dobrik, P. Nemes-Inche, G. Vertesy, Ph. Lambin, and L.P. Biro, *Phys. Rev. B* **78**, 233407 (2008).
4. A.N. Castro Neto, F. Guinea, N.M.R. Peres, K.S. Novoselov, and A.K. Geim, *Rev. Mod. Phys.* **81**, 109 (2009); K.S. Novoselov, A.K. Geim, S.V. Morozov, D. Jiang, Y. Zhang, S.V. Dubonos, I.V. Grigorieva, and A.A. Firsov, *Science* **306**, 666 (2004); Y. Zhang, Y.-W. Tan, H.L. Stormer, and P. Kim, *Nature* **438**, 201 (2005).
5. L. Liu, Yu-Xian Li, and J. Liu, *Phys. Lett. A* **376**, 3342 (2012).
6. Y. Wang, Y. Liu, and B. Wang, *Physica E* **53**, 186 (2013).
7. L. Sun, C. Fang, and T. Liang, *Chin. Phys. Lett.* **30**, 047201 (2013).
8. A. Concha and Z.Tešanović, *Phys. Rev. B* **82**, 033413 (2010).
9. J.H. Yuan, J.J. Zhang, Q.J. Zeng, J.P. Zhang, and Z. Cheng, *Physica B* **406**, 4214 (2011).
10. P.M. Krstajic and P. Vasilopoulos, *J. Phys.: Condens Matter* **23**, 135302 (2011).
11. A.M. Korol, N.V. Medvid', and S.I. Litvynchuk, *Spring. Proc. Phys.* **167**, 215 (2015).
12. А.М. Король, А.И. Соколенко, И.В. Соколенко, *ФНТ* **44**, 1025 (2018) [*Low Temp. Phys.* **44**, 803 (2018)].
13. H. Goudarzi, H. Sedghi, M. Khezelrou, Kh. Mabhouti, *Physica C* **470**, 1981 (2010).
14. S. Bhattacharjee and K. Sengupta, *Phys. Rev. Lett.* **97**, 217001 (2006).
15. H. Goudarzi and M. Khezelrou, *Physica E* **43**, 604 (2010).
16. J. Linder and A. Sundbo, *Phys.Rev. B* **77**, 064507 (2008).
17. Bumned Soodchomshom and I-Ming Tang, Rassmidara Hoonsavat, *Physica C* **469**, 689 (2009).

18. Chunxu Bai, Juntao Wang, and Yanling Yang, *Superlatt. Microstruct.* **49**, 151 (2011).
19. Bumned Soodchomshom, *J. Supercond. Nov. Magn.* **25**, 405 (2012).
20. Chunxu Bai and Yanling Yang, *Phys. Lett. A* **374**, 882 (2010).
21. Tatnatchai Suwannasit, I-Ming Tang, Rassmidara Hoonsavat, and Bumned Soodchomshom, *J. Low Temp. Phys.* **165**, 15 (2011).
22. M. Salehi and G. Rashedi, *Physica C* **470**, 703 (2010).
23. H. Goudarzi, M. Khezelrou, and T. Dezhaloud, *Physica C* **489**, 8 (2013).
24. J.P.L. Faye, P. Sahebsara, and D. Senechal, *Phys. Rev. B* **92**, 085121 (2015).
25. Rahul Nandkishore, L.S. Levitov, and A.V. Chubukov, *Nature Phys.* **8**, 158 (2012).
26. Jianfrei Zou and Guojun Jin, *EPL* **87**, 27008 (2009).
27. R. Vali and Mehran Vali, *J. Phys.: Condens. Matter* **24**, 325702 (2012).
28. Annica M. Black-Schaffer and Carsten Honerkamp, *J. Physics: Condens. Matter* **26**, 42 (2014).
29. Yu.A. Kolesnichenko, A.N. Omelyanchouk, and S.N. Shevchenko, *Fiz. Nizk. Temp.* **30**, 288 (2004) [*Low Temp. Phys.* **30**, 213 (2004)].
30. R. Mahmoodi and S.N. Shevchenko, *Fiz. Nizk. Temp.* **28**, 262 (2002) [*Low Temp. Phys.* **28**, 184 (2002)].
31. Yu.A. Kolesnichenko and A.N. Omelyanchuk, *Fiz. Nizk. Temp.* **30**, 714 (2004) **[***Low Temp. Phys.* **30**, 535 (2004)].
32. Y. Yerin and A.N. Omelyanchuk, *Fiz. Nizk. Temp.* **43**, 1263 (2017) [*Low Temp. Phys.* **43**, 1013 (2017)].
33. Liang Fu and C.L. Kane, *Phys. Rev. Lett.* **100**, 096407 (2008).
34. Yukio Tanaka, Takehito Yokoyama, and Naoto Nagaosa, *Phys. Rev. Lett.* **103**, 107002 (2009).
35. G.E. Blonder, M. Tinkham, and T.M. Klapwijk, *Phys. Rev. B* **25**, 4515 (1982).

Тунельна провідність контакту: надпровідний графен із *s*-хвильовим та *d*-хвильовим спарюванням–нормальний графен

А.М. Король

У рамках формалізму Блондера–Тинкхема–Клапвійка розраховано та проаналізовано провідність контакту: нормальний графен–надпровідний графен із *s*-хвильовим і незалежно *d*-хвильовим спарюванням. Власні функції, коефіцієнти андріївського та нормального відбивання одержані за допомогою розв'язку рівнянь Дірака–Боголюбова–де Жена. Розглянуто випадки безщільового та щільового графену для обох ситуацій: *s*-хвильового і незалежно *d*-хвильового спарювання. Показано, що характеристики даного контакту є чутливими до відношення v_{FN}/v_{FS}, де v_{FN}, v_{FS} — швидкості Фермі в нормальному та надпровідному графені відповідно. Цей результат стосується як андріївського, так і нормального відбивання. Перший з них є визначальним процесом у формуванні провідності. Зроблені висновки справедливі для довільного орієнтаційного кута *d*-хвиль. У кожного з розглянутих чотирьох випадків: *s*-, *d*-спарювання, щільового та безщільового графена, свої особливості провідності. У кожному випадку проаналізовано залежність провідності від зовнішнього електростатичного потенціалу та від енергії Фермі. Одержані результати можуть бути корисними для регулювання транспортних властивостей контакту: нормальний графен–надпровідний графен.

Ключові слова: контакт графен–надпровідний графен, андріївське та нормальне відбивання, провідність, швидкість Фермі.

Туннельная проводимость контакта: сверхпроводящий графен с *s*-волновым и *d*-волновым спариванием–нормальный графен

А.Н. Король

В рамках формализма Блондера–Тинкхема–Клапвийка рассчитана и проанализирована проводимость контакта: нормальный графен–сверхпроводящий графен с *s*-волновым и независимо *d*-волновым спариванием. Собственные функции, коэффициенты андреевского и нормального отражения получены с помощью решения уравнений Дирака–Боголюбова–де Жена. Рассмотрены случаи бесщелевого и щелевого графена для обеих ситуаций: *s*-волнового и независимо *d*-волнового спаривания. Показано, что характеристики данного контакта являются чувствительными к соотношению v_{FN}/v_{FS}, где v_{FN}, v_{FS} — скорости Ферми в нормальном и сверхпроводящем графене соответственно. Этот результат относится как к андреевскому, так и нормальному отражению. Первое из них является определяющим процессом в формировании проводимости. Сделанные выводы справедливы для произвольного ориентационного угла *d*-волн. У каждого из рассмотренных четырех случаев: *s*-, *d*-спаривания, щелевого и бесщелевоого графена, свои особенности проводимости. В каждом случае проанализирована зависимость проводимости от внешнего электростатического потенциала и энергии Ферми. Полученные результаты могут быть полезными для регулирования транспортных свойств контакта: нормальный графен–сверхпроводящий графен.

Ключевые слова: контакт графен–сверхпроводящий графен, андреевское и нормальное отражение, проводимость, скорость Ферми.